OPTOELECTRONICS AND ADVANCED MATERIALS – RAPID COMMUNICATIONS Vol. 2, No. 3, March 2008, p. 140 - 147

Analytical simulation of HgCdTe photovoltaic detector for long wavelength infrared (LWIR) applications

P. K. SAXENA, P. CHAKRABARTI*
Centre for Research in Microelectronics, Department of Electronics Engineering, Institute of Technology, Banaras Hindu University, Varanasi-221005, India

A generic model of a long-wavelength infrared photodetector based on $Hg_{1-x}Cd_xTe$ (x=0.22) narrow bandgap semiconductor has been developed to examine the potential of the device for possible application in free space optical communication at 10.6 μm. The dark current analysis of the detector has been carried out by considering all the dominant current components including tunneling. The lifetime of the carriers has been modeled by taking into the account radiative as well as non-radiative recombination processes. The analysis revealed that the current in photodetector under reverse bias is dominated by trap assisted tunneling component of the current which causes a reduction in the quantum efficiency value at low and moderate reverse bias. The noise equivalent power decreases with increase in value of the equivalent load resistance of the receiver circuit. The photodetector exhibits a dark current, $I_0 \approx 4\times10^{-6}$ A, zero-bias dynamic resistance, $R_0 \approx 10^6\,\Omega$, quantum efficiency, $\eta \approx 67$ % at 10.6 μm and noise equivalent power, (NEP) $\approx 10^{-13}$ W-Hz$^{1/2}$.

(Received February 22, 2008; accepted March 18, 2008)

Keywords: Free space optical communication, LWIR, Photodetector, HgCdTe, NEP

1. Introduction

Free space optical communication mode has received considerable attention because of its potential to serve applications requiring high bandwidth with relatively high security to eavesdropping but without the complexity of installing optical fibers. The basic advantages of free space optical communication systems include extremely high bandwidth, rapid deployment time, license and tariff free bandwidth allocation, low-power consumption, light weight, small size, low loss and no requirement of material medium through which information can be processed. It has been established that infrared region is best suited for free space optical communication [1] - [2]. The nature provides us two atmospheric transmission windows in the long wavelength infrared region at 9.6 μm and 10.6 μm which open up the possibility of exploiting infrared atmospheric transparency windows for free space optical communication. In the present study our focus is on the strategic atmospheric attenuation window at 10.6 μm because this window is more immune to adverse weather conditions e.g. fog and haze. The beam, containing billion of bits of information comprising a combination of internet messages, video images, radio signals or computer files, in Free Space Optics (FSO) systems are transmitted by laser source focused on highly sensitive ultra fast photodetector receivers. Such ultrafast high sensitive receivers operating in the long wavelength (LWIR) region deploy photovoltaic detectors based on narrow bandgap semiconductors. These receivers are equipped with telescopic lenses able to collect the photon stream and transmit digital data.

The most promising semiconductor alloys for use in LWIR region include InAsSb belonging to III-V family and HgCdTe (MCT) belonging to II-VI family. $Hg_{1-x}Cd_xTe$ semiconductor material based photodetector is the best choice for long wavelength applications due to flexibility in tailoring its bandgap. For fabrication of high-sensitivity detectors the bandgap of HgCdTe semiconductor material can be tailored over a wide infrared (from 2 μm to 30 μm) spectral range. A considerably high value of dark current at room temperature generally limits the performance of these LWIR detectors at room temperature. Surface leakage currents and tunneling currents through the space-charge region are usually held responsible for lowering the zero-bias resistance area product (R_oA) value of these photodetectors. In these devices tunneling of electrons through the space-charge region takes place under the influence of an externally applied bias, either from the valence band from the occupied traps (Wong's model) on the p-side to the conduction band on the n-side or from the trap levels to bands on the opposite side. The necessary conditions for tunneling to occur are that: (i) there are occupied energy states on the side from which the electrons tunnel and (ii) there are unoccupied states on the side to which electrons tunnel [3] - [5]. The possibility of tunneling via traps in such devices are known as trap assisted tunneling which are usually high in this tupe of device.

In the present paper the performance of photodetector has been theoretically examined considering the simplistic receiver circuit consisting of the photodetector, bias circuit and the input impedances of the following preamplifier stage.

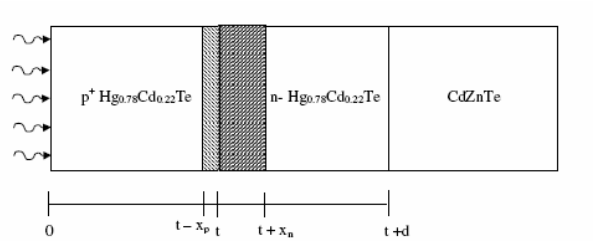

Fig. 1. Schematic diagram of p-n junction.

2. Modeling

The device under consideration consists of a p-n homojunction photodetector based on $Hg_{0.88}Cd_{0.22}Te$ material. The device is supposed to be grown on lattice matched CdZnTe substrate. The photodetector is suitably reversed biased and is followed by preamplifier having an input resistance of R_i. The schematic of the receiver is shown in Fig. 2a. A simplistic noise equivalent circuit of the receiver is shown in Fig. 2b. The I_{photo} is the d. c. value of the photon induced current, $\left\langle i_s^2 \right\rangle$ is the mean square value of the shot noise current (produced within detector) and C_J, R_J are the junction capacitance and resistance respectively. R_L is the load resistance of load resister and $\left\langle i_T^2 \right\rangle$ is the mean square value of the thermal noise current.

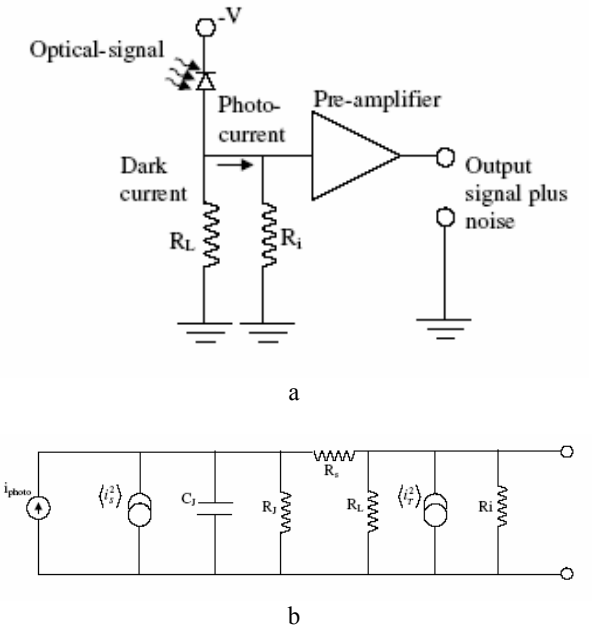

Fig. 2. a) Receiver system; b) Simplified equivalent circuit.

In practical intensity modulated direct detection (IM/DD) systems without internal gain mechanism, the minimum detectable signal is usually restricted by the shot and thermal noise components of detector and thermal noise associated with load resistance and the input resistance of the following amplifier. The minimum detectable power can be obtained as

$$\left(P_{opt}\right)_{\min} = \frac{2h\upsilon}{\eta}\left\{1+\left[1+\frac{I_{eq}}{qB}\right]^{\frac{1}{2}}\right\} \tag{1}$$

Here $$I_{eq} = I_{dark} + \frac{2kT}{qR_{eq}} \tag{2}$$

where h is the Planck's constant, ν is the frequency of light and R_{eq} is the equivalent resistance experienced by the photodetector and is given by

$$\frac{1}{R_{eq}} = \frac{1}{R_J} + \frac{1}{R_L} + \frac{1}{R_i}, \tag{3}$$

Here R_J, R_L and R_i are junction resistance of photodiode, resistance associated with external load resistor (bias resistor) and input resistance of amplifier respectively.

Dark Current Analysis

The dark current of the HgCdTe based photodetector has been modeled considering (i) the diffusion of the thermally generated carriers from the neutral regions, I_{DIFF} (ii) generation-recombination of carriers in the depletion region, I_{GR} (iii) tunneling of carriers through the barrier, I_{TUN} [7]-[11]. In present analysis, we have considered both trap assisted (TAT) and band to band tunneling (BTB) components.

$$I_{dark} = I_{DIFF} + I_{GR} + I_{TAT} + I_{BTB} \tag{4}$$

In the present structure under consideration, the diffusion of minority carriers from both p and n regions, contribute diffusion current. The minority carrier diffusion current under application of a bias voltage, V can be obtained by solving 1-D diffusion equation under appropriate boundary conditions. The diffusion current component can be obtained as

$$I_{DIFF} = (C_1 + C_2)\left(\exp\left(\frac{qV}{kT}\right) - 1\right) \tag{5}$$

where

$$C_1 = q\frac{n_i^2}{N_d}A\frac{D_p}{L_p}\frac{\frac{S_pL_p}{D_p}\cosh\left(\frac{t-x_p}{L_p}\right)+\sinh\left(\frac{t-x_p}{L_p}\right)}{\frac{S_pL_p}{D_p}\sinh\left(\frac{t-x_p}{L_p}\right)+\cosh\left(\frac{t-x_p}{L_p}\right)} \tag{6}$$

and

$$C_2 = q\frac{n_i^2 A}{N_a}\frac{D_n}{L_n}\frac{\frac{S_n L_n}{D_n}\cosh\left(\frac{d-x_n}{L_n}\right)+\sinh\left(\frac{d-x_n}{L_n}\right)}{\frac{S_n L_n}{D_n}\sinh\left(\frac{d-x_n}{L_n}\right)+\cosh\left(\frac{d-x_n}{L_n}\right)} \quad (7)$$

In the above equations, n_i is the intrinsic carrier concentration of HgCdTe, N_a and N_d are the acceptor and donor concentrations in p and n regions respectively, q is the electronic charge, D_p and D_n are the hole and electron diffusion coefficients, S_p and S_n are the surface recombination velocities of holes at p-HgCdTe/metal interface and electrons at HgCdTe/CdZnTe hetero-interface and L_p and L_n are respective diffusion lengths of holes and electrons on n- and p-side respectively. Here t and d are the thickness of p-HgCdTe and n-HgCdTe regions respectively, x_p and x_n are respectively the width of the depletion regions in p and n-regions and A is the junction area, μ_e and μ_h are the mobility of electrons and holes respectively; V is the applied potential.

The generation-recombination current component arises due to impurities and defects within the depletion region that acts as intermediate states for the thermal generation and recombination of carriers. These intermediate states are known as Shockley-Read-Hall centres. This current could be important than diffusion current, although depletion region is much less than the minority carriers diffusion length, especially at low temperature. The generation-recombination component of current density can be approximated as [11]

$$J_{GR} = \frac{qn_i WV}{(V_{bi}-V)\tau_{SRH}} \quad \text{for } V<0 \quad (8a)$$

and $$J_{GR} = \frac{2n_i WkT}{(V_{bi}-V)\tau_{SRH}}\sinh\left(\frac{qV}{2kT}\right) \quad \text{for}$$

$$V>0 \quad (8b)$$

where V_{bi} is the built-in potential, V is the applied voltage, W is the width of the depletion region which is a function of the applied voltage and n_i is the intrinsic carrier concentration and τ_{SRH} is the SRH generation-recombination lifetime.

The trap-assisted tunneling current component arises here due to electron transition from valance band to a trap level within the bandgap and then tunneling to the conduction band. These trap states are the centre of the intermediate energy levels created by the presence of impurities in the material. The trap-assisted tunneling component of current on the simple 1-D model [3]-[4] can be written as

$$I_{TAT} = \frac{2\pi^2 Aq^2 m_n^* W_c^2 N_t (V_{bi}-V)W}{h^3(E_g-E_t)}\exp\left(-\frac{\sqrt{3}WE_g^2}{8\sqrt{2}P(V_{bi}-V)}\alpha\left(\frac{E_t}{E_g}\right)\right) \quad (9)$$

$$\alpha(x) = \left\{\frac{\pi}{2}+\sin^{-1}(\pm 1\pm 2x)\pm(1-2x)[x(1-x)]^{\frac{1}{2}}\right\} \quad (10)$$

here $$x = \frac{E_t}{E_g}$$

where $W=x_p+x_n$ is the total depletion width, E_g is the energy bandgap of HgCdTe semiconductor, h is Planck's constant, V_{bi} is the build in potential, V is the applied voltage, m_n^* is effective electronic mass, N_t is the density of trap occupied by electrons. W_c and P are matrix element associated with the trap potential and interband matrix element respectively. E_t is energy corresponding to trap centres.

When the crossover of energy bands take place at high reverse bias voltage, the band to band tunneling current arises due to flow of electrons from fully occupied valance band of p-region to partially filled or empty states of conduction band of n-region. The band to band tunneling current can be obtained as [8]

$$I_{BTB} = \frac{\sqrt{2m_n^*}q^3 AEV}{4\pi^2\hbar^2 E_g^{1/2}}\exp\left(-\frac{4\sqrt{2m_n^*}E_g^{3/2}}{3qE\hbar}\right)$$

where, $$E = \left[\frac{2q}{\varepsilon_0\varepsilon_s}\left(\frac{E_g}{q}\pm V\right)\frac{n_0 p_0}{n_0+p_0}\right]$$

The inverse of resistance due to dark currents can be directly obtained by differentiating dark currents with respect to voltage. Thus

$$R_J(V) = \left(\frac{dI}{dV}\right)^{-1} \quad (13)$$

The net value of dynamic resistance of photodiode can be obtained as

$$\frac{1}{(R_J)_{NET}} = \frac{1}{(R_J)_{DIFF}}+\frac{1}{(R_J)_{GR}}+\frac{1}{(R_J)_{TAT}}+\frac{1}{(R_J)_{BTB}} \quad (14)$$

Modeling of carrier lifetime

In order to accurately compute the drift and diffusion components of current, it is necessary to model the lifetime of minority carriers considering all the possible recombination mechanisms. In the present lifetime modeling, we have considered bulk recombination processes in HgCdTe to involve radiative recombination and two non-radiative recombination mechanisms. The direct band-to-band photon assisted recombination is radiative recombination and the phonon assisted

recombination processes consists of Auger and Shockley-Read-Hall (SRH) recombination mechanisms which are non-radiative recombination processes. The modeling of the radiative recombination process is straightforward. For direct bandgap HgCdTe semiconductors, the lifetime of carriers due to radiative recombination for low level injection can be approximated as [13]-[14]

$$\tau_{RAD} = \frac{n_i^2}{G_R\left(n_0 + p_0\right)} \tag{15}$$

$$G_R = 5.8\times10^{-13} n_i^2 \varepsilon_\infty^{1/2}\left(\frac{m_0}{m_n^* + m_p^*}\right)^{\frac{3}{2}}\left(1+\frac{m_0}{m_n^*}\right)\left(\frac{300}{T}\right)^{\frac{3}{2}}\left(E_g^2 + 3kTE_g + 3.75k^2T^2\right) \tag{16}$$

where G_R is the thermal equilibrium spontaneous generation rate of the HgCdTe semiconductor material and n_0 and p_0 are the electron and hole concentrations respectively in the region under thermal equilibrium. E_g is the band gap in eV, m_n^* and m_p^* are the effective mass for electrons and holes.

The non-radiative Auger recombination is quite complex. It is an important mechanism in determining the performance of light-emitting devices and infrared detectors made from narrow-gap semiconductors. A semiconductor with a single conduction band and heavy-hole and light-hole valence band there can occur at least ten different types of Auger transitions. Out of these transitions, the two most significant transitions that occur at the minimum threshold energy ($E_T \approx E_g$) are the Auger-1 or CHCC (involving two conduction band electrons and a heavy hole) and Auger-7 or CHLH (involving one conduction band electron and one heavy hole and one light hole). The former is generally dominant in n-type material and the later in p-type material. The net Auger recombination lifetime of the carriers can thus be written as

$$\frac{1}{\tau_{AU}} = \frac{1}{\tau_{A-1}} + \frac{1}{\tau_{A-7}} \tag{17}$$

The Auger-1 recombination process involves the direct band-to-band recombination of a conduction band electron with a heavy hole and excitation of another electron in conduction band, dominant in n-type HgCdTe material. The intrinsic lifetime for the Auger-1 process is

$$\tau_{A1}^{(i)} = 3.8\times10^{-18}\varepsilon_s^2\frac{m_0}{m_n^*}\left(1+\mu\right)^{1/2}\left(1+2\mu\right)\times\left(\frac{E_g}{kT}\right)^{3/2}\exp\left(\frac{1+2\mu}{1+\mu}\frac{E_g}{kT}\right)\left|F_1F_2\right|^{-2} \tag{18}$$

where μ is the ratio of electron to hole effective masses, ε_s is the high-frequency dielectric constant, $|F_1F_2|$ is the overlap integral of the Block functions (values ranging from 0.1 to 0.3). The Auger-1 lifetime is

$$\tau_{A1} = \frac{2n_i^2}{\left(n_0 + p_0\right)n_0}\tau_{A1}^{(i)} \tag{19}$$

where p_0 and n_0 are the thermal equilibrium concentration for holes and electrons respectively.

The Auger-7 process involves the direct band-to-band recombination of a conduction band electron with a heavy hole and excitation of an electron of an electron from light hole band to heavy hole band. The Auger-7 lifetime is

$$\tau_{A7} = \frac{2n_i^2}{\left(n_0 + p_0\right)p_0}\gamma\tau_{A1}^{(i)} \tag{20}$$

here $\gamma = \tau_{A7}^i / \tau_{A1}^i$ depends on composition 'x' of HgCdTe material and temperature.

The computation details of the various components of Auger recombination lifetime are amply discussed elsewhere [13].

The lifetime of carriers due to Shockley-Read-Hall recombination can be modeled in terms of trap density and capture cross-section as

$$\tau_{SRH} = \frac{1}{\sigma N_T v_{th}} \tag{21}$$

where N_T is the SRH trap density, σ is the capture cross-section and v_{th} is the thermal velocity of the minority carriers in the active region, given by

$$v_{th} = \sqrt{\frac{3kT}{m_n^*}} \tag{22}$$

m_n^* is the effective mass of electrons in the active region.

The effective lifetime of the carriers in the active region can be obtained as

$$\frac{1}{\tau_{eff}} = \frac{1}{\tau_{RAD}} + \frac{1}{\tau_{AU}} + \frac{1}{\tau_{SRH}} \tag{23}$$

Quantum Efficiency

The quantum efficiency (η) of a p-n junction photodetector has generally three major components. These components arise from the contribution of the three regions e.g., neutral n-region (η_n), neutral p-region (η_p) and the depletion region (η_{dep}). The optical generation rate of electron-hole pairs, as a function of distance x from the surface can be written as [15] - [16]

$$G(x) = \frac{\alpha(\lambda)(1-R)P_{opt}}{Ah\nu}\exp\left(-\alpha(\lambda)x\right) \tag{24}$$

where $\alpha(\lambda)$ is the optical absorption coefficient of the material which is a function of wavelength λ, R is the

Fresnel reflection coefficient at the entrance, P_{opt} is the incident optical power, ν is the frequency of radiation and A is the device area. The quantum efficiency components can be obtained as

$$\eta_n = \frac{(1-R)\,\alpha L_p}{\alpha^2 L_p^2 - 1}\exp(-\alpha(t+x_n))\left[\frac{(\gamma_p - \alpha L_p)\exp(-\alpha(d-x_n)) - \left[\gamma_p \cosh\left(\frac{d-x_n}{L_p}\right) + \sinh\left(\frac{d-x_n}{L_p}\right)\right]}{\gamma_h \sinh\left(\frac{d-x_n}{L_p}\right) + \cosh\left(\frac{d-x_n}{L_p}\right)} + \alpha L_p\right]$$

25)

$$\eta_p = \frac{(1-R)\,\alpha L_n}{\alpha^2 L_n^2 - 1}\left[\frac{\alpha L_n + \gamma_n - \exp\left(-\alpha\left(t-x_p\right)\right)\left[\gamma_n \cosh\left(\frac{t-x_p}{L_n}\right) + \sinh\left(\frac{t-x_p}{L_n}\right)\right]}{\gamma_n \sinh\left(\frac{t-x_p}{L_n}\right) + \cosh\left(\frac{t-x_p}{L_n}\right)} - \alpha L_n \exp\left(-\alpha\left(t-x_p\right)\right)\right]$$

(26)

where L_p and L_n are the hole and electron diffusion lengths in n and p regions respectively. $\gamma_n = S_n L_n / D_n$ and $\gamma_p = S_p L_p / D_p$ are the ratio of surface to bulk recombination velocity in p and n regions respectively.
The contribution of the photo-generated carriers in the depletion region to the total quantum efficiency can be obtained as

$$\eta_{dep} = (1-R)\left\{\exp\left(-\alpha\left(t-x_p\right)\right) - \exp\left(-\alpha\left(t+x_n\right)\right)\right\} \tag{27}$$

The net quantum efficiency can be written as

$$\eta = \eta_n + \eta_p + \eta_{dep} \tag{28}$$

Photocurrent

In the present analysis the incident light is assumed to be intensity modulated. The incident optical power for a single tone modulation is assumed to be of the form

$$P(t) = P_{opt}\left(1 + \mu \cos 2\pi f_m t\right) \tag{29}$$

where f_m is the modulating signal frequency and μ is the index of modulation.

The dc component of the photocurrent generated in the photodetector can be obtained as

$$I_{photo} = \frac{q\eta P_{opt}}{h\upsilon} \tag{30}$$

Here η is the quantum efficiency of the photodetector and $h\upsilon$ is the photon energy of the incident light beam.

The root mean square value of the signal current can be obtained as

$$i_{photo} = \frac{q\eta P_{opt}}{\sqrt{2}h\upsilon}\mu \tag{31}$$

Noise current modeling

The shot noise in photodetector is generated out of thermally generated carriers which are injected randomly. In presence of illumination, there is generation of excess carriers due to absorption of light in the material. This photogeneration is random in nature and manifests in the form of additional shot noise current. In presence of the received light, the mean square value of the shot noise current can be obtained as

$$\left\langle i_S^2 \right\rangle = 2q\left(I_{photo} + I_{dark}\right)B \tag{32}$$

where B is the bandwidth.

The mean square value of the thermal noise associated with the photodetector can be express as

$$\left\langle i_T^2 \right\rangle = \frac{4kT}{R_{eq}}B \tag{33}$$

where
$$\frac{1}{R_{eq}} = \frac{1}{R_J} + \frac{1}{R_L} + \frac{1}{R_i}, \tag{34}$$

Here R_J, R_L and R_i are dynamic resistance of photodiode junction, resistance associated with external load resistor and input resistance of amplifier respectively.

The signal to noise ratio can be expressed as

$$\left(\frac{S}{N}\right)_{power} = \frac{\frac{1}{2}\left(q\eta P_{opt}/h\upsilon\right)}{2q\left(I_{photo} + I_{dark}\right)B + 4kTB/R_{eq}} \tag{35}$$

here k is the Boltzmann constant and T is the temperature.

The noise equivalent power (NEP) is defined as the signal power, P_{opt} necessary to produce the signal noise ratio of unity at the output for unit bandwidth (B=1Hz). The root mean square value of the noise equivalent power can be obtained as

$$NEP = \frac{\left(P_{opt}\right)_{\min}}{\sqrt{2}} \tag{36}$$

3. Results and discussion

Numerical computations have been carried out on p-$Hg_{0.88}Cd_{0.22}Te$/n-$Hg_{0.88}Cd_{0.22}Te$ photodetector at 77K for operation at 10.6 μm. The light has been assumed to be incident on the top p-$Hg_{0.88}Cd_{0.22}Te$ side of the photodetector. The photons with energy higher than the energy gap create electron-hole pairs in p and n region.

Various parameters used in the theoretical computations are listed in Table 1. The absorption coefficient of HgCdTe has been computed as a function of wavelength by using modified Urbach's rule [17] – [18].

Table. 1. Parameters used for calculation.

Parameters used	Values
E_g	$(-0.302+1.93x-0.81x^2+0.832x^3+5.35\times10^{-4}(1-2x)T)$ eV
Δ	0.96 eV
N_t	2.1×10^{19} m^{-3}
σ	4.7619×10^{-20} m^2
N_d	3.5×10^{20} m^{-3}
N_a	9.3×10^{21} m^{-3}
W_c^2	3×10^{-67} J^2m^3
P	0.83 eV
A	7.3×10^{-9} m^2
ε_s	12.5 ε_0
m_0	9.1×10^{-31} kg
m_n^*	$m_0(1+2m_0P^2(E_g+2\Delta/3)/(h^2E_g(E_g+\Delta)))^{-1}$
m_p^*	0.55 m_0
S_p	10 m/s
S_n	10^4 m/s
R_L	0.5-20 MΩ
R_i	4.5 MΩ

Results of numerical computations reveal that the trap assisted tunneling component of current in HgCdTe photodetector is dominant even at low and moderate reverse bias while the diffusion component of current becomes dominant at forward bias. The different dark current components of the photodetector have been calculated using the theoretical model. The dependence of dynamic resistance of photodetector on the applied voltage has been quantitatively estimated and validated with the experimental results. For the model validation, separate calculation has been carried out at 77 K for operation at 10 μm. The validated model is then applied to electrically and optically characterize the HgCdTe based photodetector for operation at 10.6 μm.

Fig. 3 illustrates the variation of the total dynamic resistance contributed by diffusion, generation-recombination, trap assisted tunneling and band-to-band tunneling components (different components have not been shown here) with applied voltage. We have applied our proposed model to estimate the total dynamic resistance at 77 K for operation at 10 μm. The results obtained, using model is in fairly good agreement with the experimental result given in reference [6]. The curve of total dynamic resistance increases linearly in moderate and low reverse bias voltage upto zero reverse bias, showing linear dependence of total dynamic resistance on reverse bias voltage in 10^5-10^6 Ω range of total dynamic resistance. The total dynamic resistance, in reverse direction is dictated by trap assisted tunneling component. The total dynamic resistance has the maximum value of 10^6 Ω near zero bias voltage.

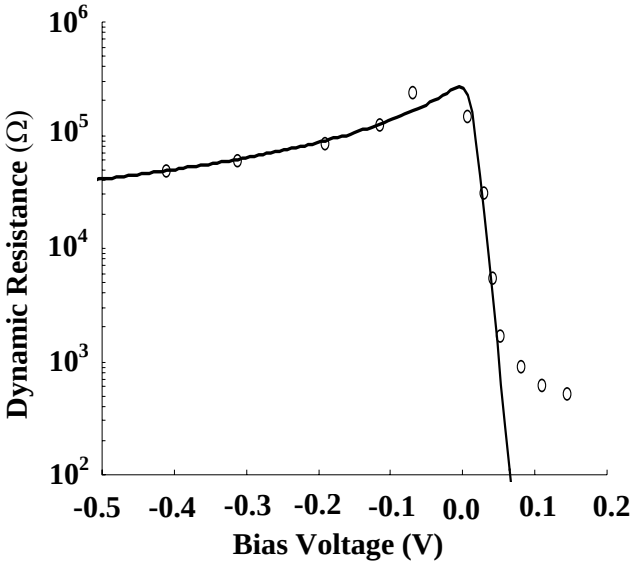

Fig. 3. Variation of dynamic resistance with bias voltage (Theoretical model and experimental results reported in ref. 6) for operation at 10 μm.

Fig. 4 depicts the variation of different components of dark current (e.g. diffusion (DIFF), generation-recombination (GR) and tunneling) and total dark current of the photodetector with applied reverse bias voltage for operation at 10.6 μm. The variation of total dark current with applied reverse bias indicate that the trap assisted tunneling (TAT) component of dark current, dominate in moderate and low reverse bias voltage while in forward bias direction total dark current is dominated by diffusion component of dark current. In moderate to low reverse bias direction, the total dark current is almost constant and has the minimum value 4×10^{-6} A at near zero bias. The contribution of band-to-band tunneling (BTB) and generation-recombination (for an SRH trap density of 10^{19} m^{-3}) components of dark current, in the total dark current in reverse direction is almost negligible.

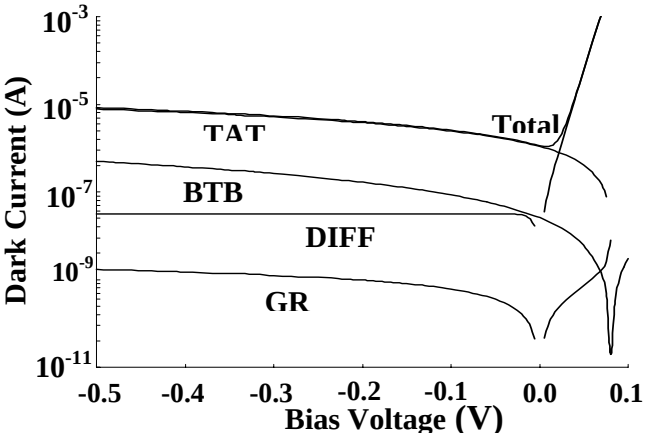

Fig. 4. Variation of different components of dark current with bias voltage.

The variation of quantum efficiency, as a function of operating wavelength, of photodetector at 77 K is shown in Fig. 5. It is seen that homojunction p- $Hg_{0.88}Cd_{0.22}Te$/n-$Hg_{0.88}Cd_{0.22}Te$ photodetector under consideration has a peak of efficiency near 10.6 μm wavelength, which is desirable. The maximum quantum efficiency exhibited by the device is 67%. The quantum efficiency falls very fast beyond the cut-off wavelength (λ_c=10.6 μm). In shorter wavelength region quantum efficiency falls very slowly, because of high absorption of photons in the neutral region.

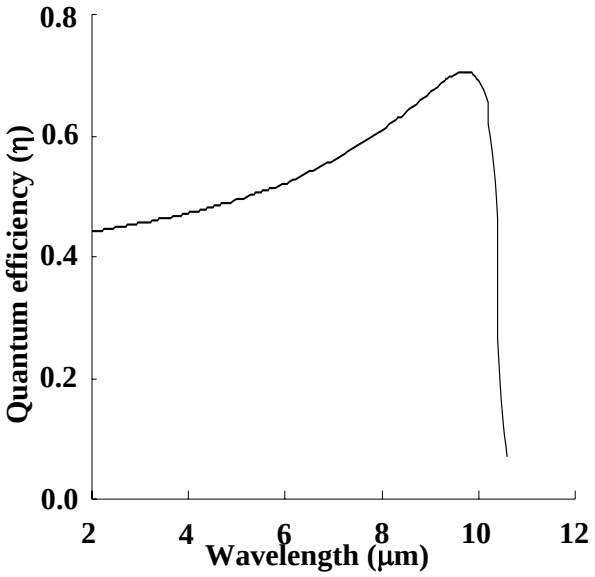

Fig. 5. Variation of quantum efficiency with operating wavelength.

The variation of noise equivalent power of the receiver circuit with equivalent resistance experienced by detector is shown in Fig. 6. In noise equivalent power computation, a simplistic noise model has been considered. In the shot noise modeling, we have taken only shot noise generated by the photodetector only. The shot noise generated by the following amplifier stage has not been taken into consideration. The photodetector exhibits a NEP of $\approx 10^{-13}$ W-Hz$^{1/2}$ for an equivalent resistance of 0.1 MΩ. The NEP value improves as the equivalent resistance is increased. A significant improvement in NEP value is obtained when the equivalent load resistance increases beyond 0.1 M.

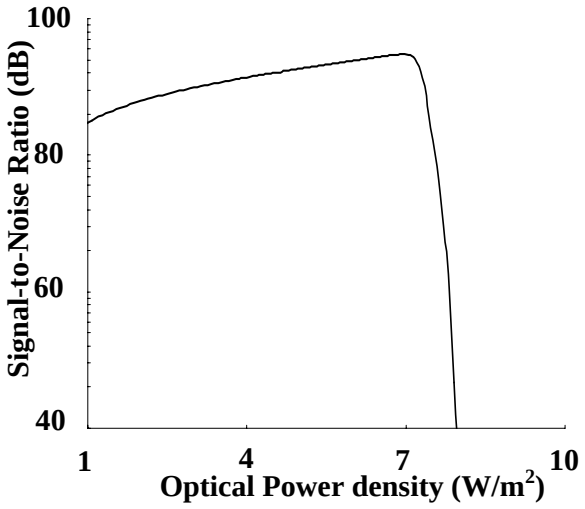

Fig. 6. Variation of Noise-equivalent-power with Equivalent load resistance.

Fig. 7 shows the variation of signal-to-noise ratio with incident optical power density. The variation of signal-to-noise ratio at low incident optical power density indicates that the shot noise produced within the device is low. The signal-to-noise ratio increases upto a particular value of incident optical power density, where the device has ultra low noise current. The graph shows a sudden decrease in signal-to-noise ratio at high incident optical power density near 7×10^5 W/m^2, because in this region the shot noise associated with photogenerated carriers override the signal current generated at the output by the received optical power. The signal-to-noise ratio associated with receiver exhibits peak value of 90 dB for an incident optical power density of value 7×10^5 W/m^2.

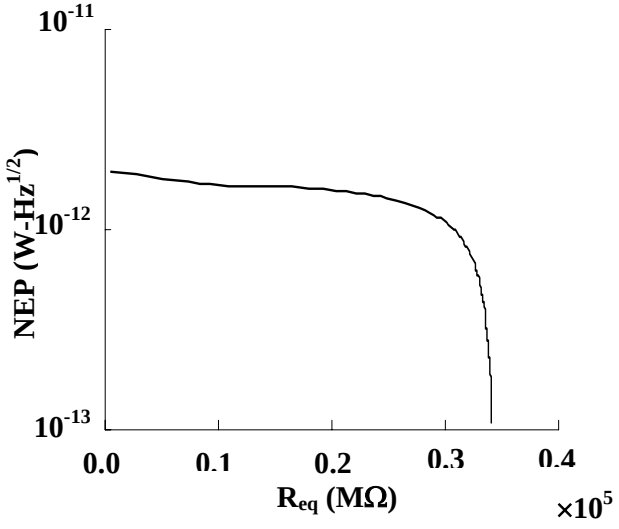

Fig. 7. Variation of signal-to-noise ratio with received optical power density.

4. Conclusion

In this paper a simplistic noise model of a receiver based on an HgCdTe photodetector has been developed for the proposed application in free space optical communication system. The key photopdetector parameters have been theoretically analyzed in order to estimate the noise equivalent power. The study reveals that the proposed photodetector can be effectively used in the receiver of a free space optical communication system at 10.6 μm. A more rigorous analysis of the receiver considering the noise components associated with the pre-amplifier is currently underway.

References

[1] Haim Manor, Shlomi Arnon, Applied Optics **42,** 4285-4294 (2003).
[2] Z. Bielecki, W. Kolosowski, E. Sedek, M. Borejko, Proc. TELSIKS-2003, pp71-74, held at Nis during Oct. 1-3, (2003).
[3] A. Unikovski, Y. Nemirovski, Appl. Phys. Lett. **61**, 330-332 (1992).
[4] David Rosenfeld, Gad BahirIEEE Trans. Electron Devices**, ED-39**, 1638-1645 (1992).
[5] J. Y. Wong, IEEE Trans. Electron Devices**, ED-27**, 48-57 (1980).
[6] T. Nguyen, C. A. Musca, J. M. Dell, J. Antoszewski, L. Faraone, Journal of Electronic Materials **32**, 1-7 (2003).
[7] V. Gopal, S. K. Singh, R. M. Mehra, Infrared Physics and Technology, **43**, 317-326 (2002).
[8] J. V. Gumenjuk-Sichevskaya, F. F. Sizov, Semicond. Sci. Technol, **14**, 1124-1131 (1999).
[9] Vishnu Gopal, Sudha Gupta, R. K. Bhan, R. Pal, P. K. Chaudhary, V. Kumar, Infrared Physics and Technology*,* **44**, 143-152 (2003).
[10] A. Rogalski, K. Adamiec, J. Rutkowski:, SPIE Press, Bellingham, USA, 2000.
[11] P. Chakrabarti, P. K. Saxena, R. K. Lal, International Journal of Infrared and Millimeter waves, **27**, 1119-1132 (2006).
[12] R. Schoolar, S. Price, J Rosbeck, J. of Vacuum Science and Tech. B, **10**, 1507-1514 (1992).
[13] V. C. Lopes, A. J. Syllaios, M. C. Chen, Semicond. Sci. Technol. **8**, 824-841 (1993).
[14] S. H. Shin, J. M. Arias, M. Zandian, J. G. Pasko, R. E. DeWames, Appl. Phys. Lett. **59**, 2718-2720 (1991).
[15] Y. Tian, B. Zhang, T. Zhan, H. Jiang, Y. Jin, IEEE Trans. Electron Dev., **ED-47**, 544-551 (2000).
[16] P. Chakrabarti, A. Krier, A. F. Morgan, IEEE Trans. on Electron Devices, **ED-50**, 2049-2058 (2003).
[17] J. Chu, Z. Mi, D. Tang, Infrared Phys. **32**, 195-211 (1991).
[18] J. Chu, Z. Mi, D. Tang, J. Appl. Phys. **71**, 3955-3961 (1992).

*Corresponding author: pchakra@bhu.ac.in